CHEMISTRY OF MATERIALS

Article

pubs.acs.org/cm

Unified Synthetic Approach to Silver Nanostructures by Galvanic Displacement Reaction on Copper: From Nanobelts to Nanoshells

Ran Liu and Ayusman Sen*

Department of Chemistry, The Pennsylvania State University, University Park, Pennsylvania, 16802

Supporting Information

ABSTRACT: We report a unified nontemplate approach to a variety of silver nanostructures, including nanobelts, dendrites, nanodisks, and nanoshells. The growth of these silver nanostructures occurs by galvanic displacement initiated by short-circuited nanobatteries formed between the copper nano/microparticles and protruding silver "seeds" on their surface. The silver nanostructures share analogous structural features because they develop from very similar silver seed crystals during their early growth stage. Transmission electron microcopy (TEM) studies reveal essentially identical electron diffraction patterns and crystal structures through the different growth stages. The formation of different silver nanostructures can be systematically controlled, for example, by varying the size of the copper particle as well as the identity and concentration of the starting silver(I) species.

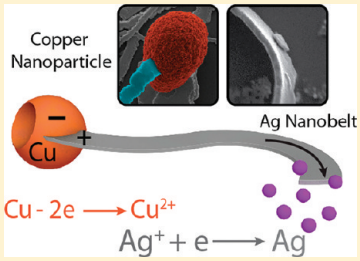

KEYWORDS: *galvanic displacement, silver nanostructures, nanobelt, dendrite, nanodisk, core−shell*

INTRODUCTION

Silver nanostructures including nanowires,[1−8] nanodisks[9−14] and nanoshells[15,16] have attracted considerable attention as a result of their unique electrical and optical properties and biocompatibility.[1−8,10−13,17−26] For example, one-dimensional (1-D) silver nanowires have been used to fabricate transparent conductive electrodes.[27−29] 2-D silver nanoplates synthesized on semiconductor substrates can exhibit strong surface enhanced plasmon resonance.[9,30] Silver nanoshells coated on the cobalt nanoparticles have been used as enhanced magneto-optical materials.[15] Typical synthetic methods for silver nanostructures involve the reduction of the Ag(I) ion (chemically,[1,2,6−8,18,21,25,31] photochemically,[3−5] and electrochemically[3−5]) in the presence of a template scaffold[2−5,8,10,12,17,21,25] or with the assistance of capping agents[1,6,7,11,13,18,20] or onto existing nanostructures.[15,16] Indirect methods, such as the transformation of existing silver-based nanomaterials into other desired silver nanostructures by thermal,[23] ultrasonic,[24] and chemical reduction[19] have also been described.

Galvanic displacement has also been applied to synthesize silver nanostructures (e.g., silver nano-inukshuks on germanium,[22] microscaled silver dendrites on aluminum surface,[32] nanoplates,[14] and nanowire[33] on semiconductor substrate[9,34,35]), as well as other types of nanomaterials (e.g., lead nanowires on zinc foil[36] and Bi_2Ti_3,[37] platinum nanotubes,[38] and gold nanocages[39,40] over existing nanostructures). However, the formation of 1-D silver nanostructures by galvanic displacement reaction has rarely been reported.

Here, we report a unified synthetic approach to silver nanostructures (especially 1-D silver nanobelts) by galvanic displacement[9,22,32,36−38] initiated by short-circuited nanobatteries formed between the copper nano/microparticles and protruding silver "seeds" on their surface. The current study provides a systematic approach to the synthesis of various silver nanostructures: by rationally varying the size of the copper particle, the identity and concentration of the starting silver(I) species, silver structures ranging from nanoshells → nanodisks → nanobelts → dendrites can be obtained (Scheme 1). The silver nanostructures share analogous structural features because they develop from very similar silver seed crystals during their early growth stage. Transmission electron microscopy (TEM) studies reveal essentially identical electron diffraction patterns and crystal structures through the different growth stages. We also describe the correlation between the silver nanostructures and the cell potentials involved in the displacement reactions. The growth of the nanobelts has been visualized and monitored in real time. The process requires no template, surfactant, or capping agent, resulting in clean surfaces for the nanostructures.

RESULTS AND DISCUSSION

Figure 1a shows the scanning electron microscopy (SEM) image of a network of Ag nanobelts grown from commercial copper nanoparticles (500 nm) (Figure S1a in the Supporting Information) in 5 mM silver nitrate solution. Figure 1b is the side view of a Ag nanobelt showing the surface morphology. Figure 1c shows a very long Ag nanobelt (approximately 40 μm) linked to an incompletely consumed copper nanoparticle. Figure 1d illustrates a plausible growth mechanism for silver nanobelts. The initial galvanic displacement reaction between the copper particle and aq $AgNO_3$ solution results in the

Received: June 21, 2011
Revised: November 15, 2011
Published: November 22, 2011

   dx.doi.org/10.1021/cm2017714 | *Chem. Mater.* 2012, 24, 48−54

Scheme 1. Various Ag Nanostructures Controlled by Tuning Copper Particle Sizes and $AgNO_3$ Concentrations

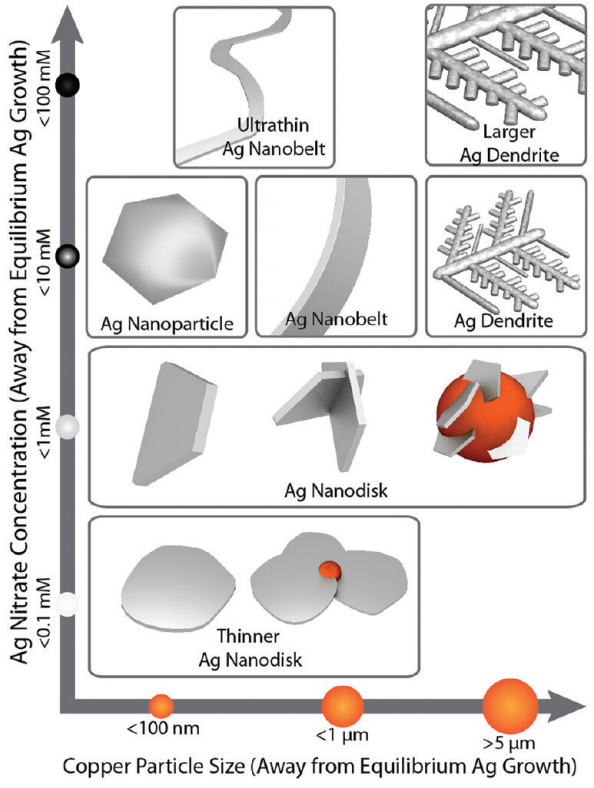

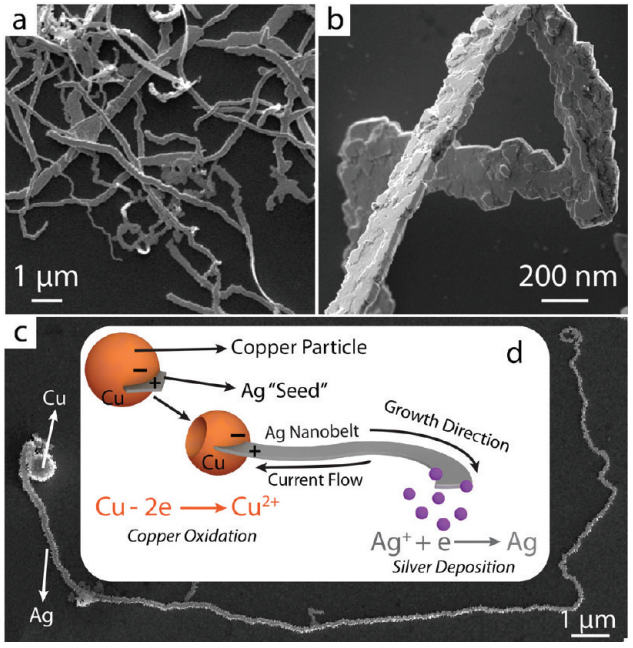

Figure 1. (a–c) SEM images of Ag nanobelts grown from 500 nm copper nanoparticle in 5 mM $AgNO_3$ in 5 min. (d) Growth mechanism of silver nanobelts.

formation of protruding Ag seeds on the surface of the copper (Figure 6). The resultant Cu–Ag junctions function as short-circuited nanobatteries; the copper end serves as the anode and is oxidized to copper ions (see Figure S2 in the Supporting Information for an incompletely oxidized copper particle), while silver ions from solution are reduced to metallic silver and preferentially deposited on the tips of the cathodic Ag seeds. The redox reaction between metallic copper and Ag^+ ion generates an electric current that supports the continued growth of the cathodic end of the nanobattery into silver nanobelts. Consistent with this hypothesis, silver was found to be selectively deposited from aq $AgNO_3$ onto the Ag segment of segmented Cu–Ag nanorods (Figure S3 in the Supporting Information). The silver nanobelt becomes gradually thinner as it grows and stops when the copper nanoparticle is completely consumed. The Ag nanobelts shown in Figure 1a have different widths because they represent different growth stages. As discussed later, different silver concentrations affect the potential difference and the current directionality between Cu–Ag junctions, resulting in the formation of different morphologies of silver nanostructures.

The TEM image of a silver nanobelt is shown in Figure 2a. The silver nanobelt appears to be "electron transparent",

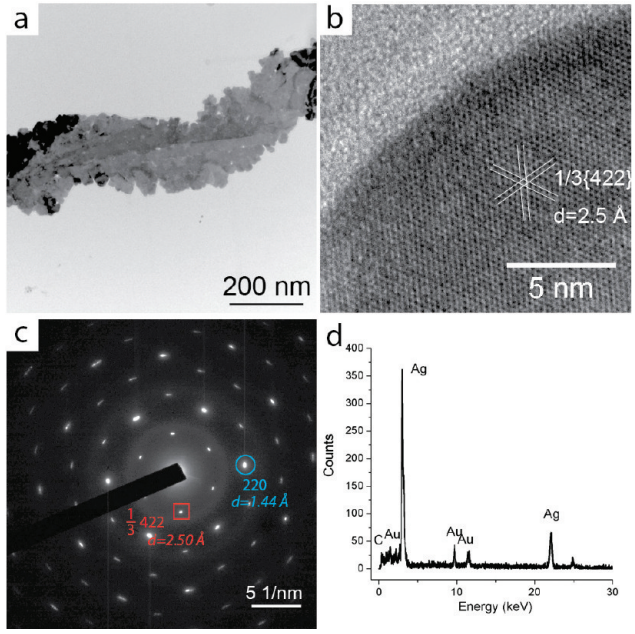

Figure 2. (a–c) TEM characterizations of Ag nanobelts synthesized from 500 nm copper nanoparticle in 5 mM $AgNO_3$ in 5 min. (d) EDS elemental analysis of a single Ag nanobelt.

suggesting that it is quite thin. The high-resolution TEM (HRTEM) of the edge of this Ag nanobelt is shown in Figure 2b and matches the 3 × {422} superlattice fringes from the Ag [111] orientation. Figure 2c shows the selected area electron diffraction (SAED) pattern of the silver nanobelt. The intense spots in the [111] zone axis are allowed {200} Bragg reflection (e.g., blue circle, corresponding to the lattice spacing of 1.44 Å). The additional relatively weak spots in the diffraction pattern correspond to the normally forbidden 1/3 {422} Bragg reflection (e.g., red square, with the lattice spacing of 2.50 Å) of fcc Ag. The HRTEM and SAED pattern of Ag can be explained by a Ag (111) stacking fault model[41] and matches well with reported Ag nanodisk structures.[41,42] The energy-dispersive X-ray spectroscopy (EDS) elemental analysis further confirms that the nanobelt is composed of pure silver phase (Figure 2d). (The Au signal is from the TEM grid.)

Parts a–c of Figure 3 show snapshots of the growth of a silver nanobelt in real time (see also the video in the Supporting Information). Based on the direct visualization of

dx.doi.org/10.1021/cm2017714 | Chem. Mater. 2012, 24, 48–54

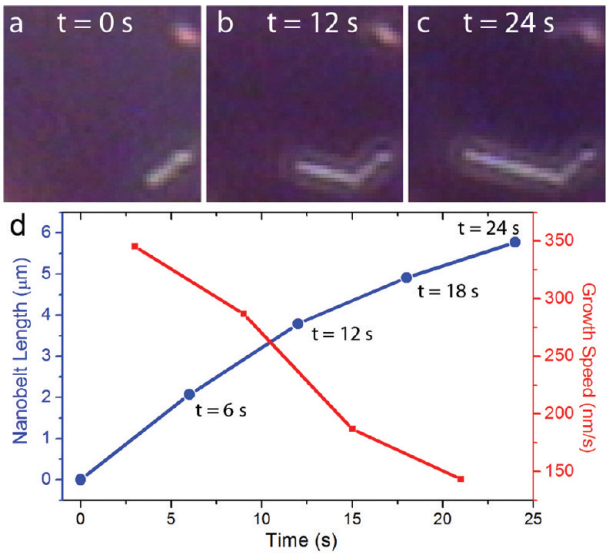

Figure 3. (a–c) Cropped frames of a growing silver nanobelt at different time stamps in 5 mM silver nitrate solution. (d) Nanobelts length and growth rate versus time.

the process, the growth rate of silver nanobelt over different time intervals can be calculated. The average growth rate in the first 6 s is 345 nm/s and decreases to 287, 187, 143 nm/s in the successive 6 s periods (Figure 3d). Some silver nanobelts decrease in thickness as they grow (Figure 1c). The decrease in the nanobelt thickness and growth rate may be due to (a) the gradual depletion of the copper particle and/or (b) the decrease in current density with increasing resistance of the elongating silver nanobelt. The current density in the nanobattery can be estimated from the growth rate of the silver nanobelts based on Faraday's law. The charge associated with silver nanobelt growth over t s is given by

$$Q_{\text{belt}} = \frac{\rho s v F t}{M} \tag{1}$$

where ρ is the density of silver, s is the cross-sectional area of the nanobelt, v is the growth rate, F is the Faraday constant, and M is the atomic weight of silver. The charge passed through the nanobattery is

$$Q_{\text{battery}} = ist \tag{2}$$

Assuming that the charge passed is all used to synthesize the Ag nanobelt, $Q_{\text{belt}} = Q_{\text{battery}}$, the current density is given by

$$i = \frac{\rho v F}{M} \tag{3}$$

From eq 3 and Figure 3d, the current density for the first 6 s is estimated to be approximately 320 mA/cm^2, which is quite high. Such high current density may arise from the high reactive surface area of copper nanoparticles.

As illustrated in Scheme 1, our approach allows the directed synthesis of a variety of silver nanostructures, in addition to nanobelts, by simply varying the Ag ion concentration and the size of the starting copper nano/microparticle. Higher silver ion concentrations and larger copper particles lead to kinetically controlled one-dimensional structures (belts and dendrites). Slowing the growth of the structure by reducing the silver ion concentration or the size of the copper particles results in more thermodynamically controlled two-dimensional structures (disks).

Figure 4 shows the nanostructures formed as a function of $AgNO_3$ concentration. When a low concentration of $AgNO_3$

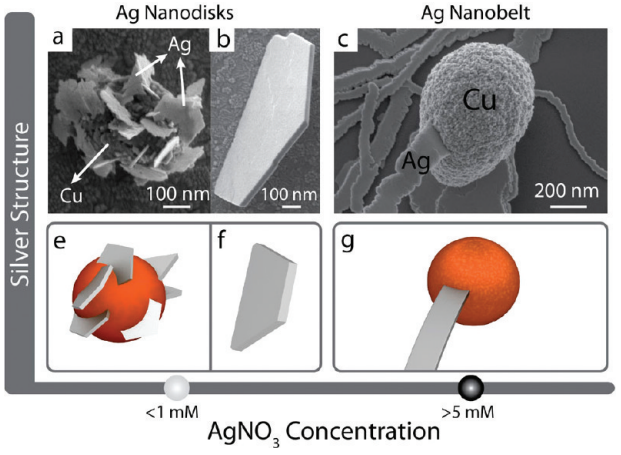

Figure 4. Ag nanostructures formed as a function of $AgNO_3$ concentration: (a, e) 0.1 mM [Ag^+] and 500 nm Cu particle for 30 s, (b, f) 0.5 mM [Ag^+] and 200 nm Cu nanoparticle for 2 min, (c, g) 5 mM [Ag^+] and 500 nm Cu nanoparticle for 1 min.

(<1 mM) is used, Ag nanodisks are formed (Figure 4 a, e and b, f). Moreover, lowering the concentration of $AgNO_3$ results in thinner disks. Very small, thin Ag nanoflakes are formed with a $AgNO_3$ concentration of 0.1 mM (Figure 4a, e). Submilimolar $AgNO_3$ (0.5 mM) leads to the formation of larger and thicker, free-standing Ag nanodisks (Figure 4b, f). Similar rules apply for the silver nanobelt formation. When 5 mM $AgNO_3$ is employed, wider Ag nanobelts (ca. 200 nm width) are formed (Figure 4c, g). When a very high concentration of $AgNO_3$ (100 mM) is utilized, ultrathin Ag nanobelts with width less than 50 nm are formed (Figure S4 in the Supporting Information).

On the basis of the relationship between Gibbs free energy and the electrochemical cell potential (eq 4), as well as the Nernst equation (eq 5), it is clear that changing the Ag^+ concentration will affect the thermodynamic driving force for the galvanic displacement reaction and can possibly lead to the formation of different silver nanostructures.

$$\Delta G = -nFE \tag{4}$$

$$E = E^0 - \frac{0.05916V}{n}\log_{10}\frac{a_{\text{Red}}}{a_{\text{Ox}}} \tag{5}$$

As shown in Figure 5a, we have measured the cell potential with varying Ag^+ concentrations. As expected, and in accordance with theory, decreasing the concentration of $AgNO_3$ from 10 mM to 0.1 mM, results in a drop in the cell potential from 0.35 to 0.24 V. At the same time, different silver nanostructures are generated (Figure 4). Higher cell potential and a higher thermodynamic driving force leads to a stronger directionality in the growth of the silver nanostructure, such as 1-D nanobelts (kinetic control). A lower cell potential results in the formation of 2-D silver nanodisks that are less protruding and more restricted to the copper surface (thermodynamic control). On the basis of this trend, we anticipated that a further lowering of the cell potential should result in the formation of silver nanoshells that uniformly cover the copper surface. When a 5 mM solution of $[Ag(S_2O_3)]^{2-}$ was employed,

dx.doi.org/10.1021/cm2017714 | Chem. Mater. 2012, 24, 48–54

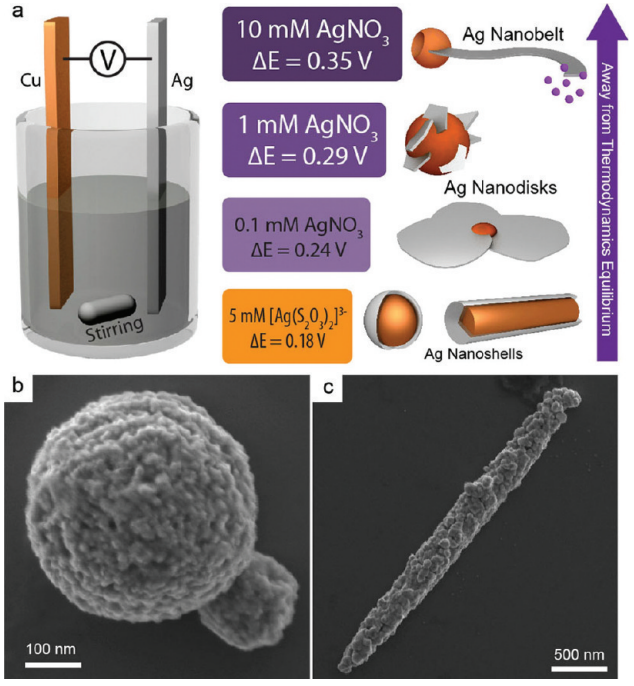

Figure 5. (a) Correlation between copper/silver cell potential and Ag nanostructures in different electrolyte (b) and (c) uniform Ag nanoshell formation on the copper microparticle (commercially available) and copper nanowire (template synthesized).

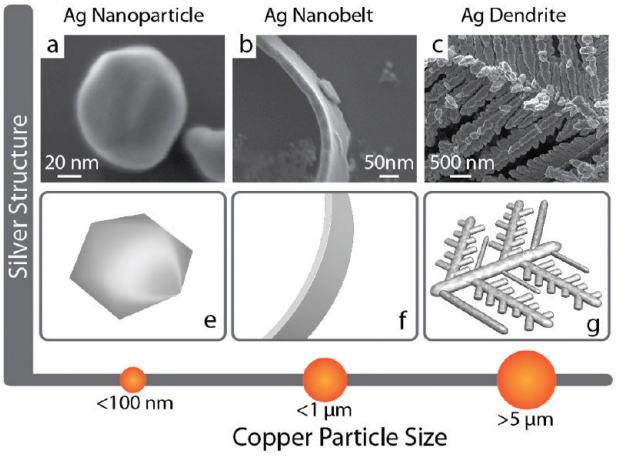

Figure 6. Ag nanostructures formed as a function of copper particle size at a fixed $AgNO_3$ concentration (5 mM) in 5 min.

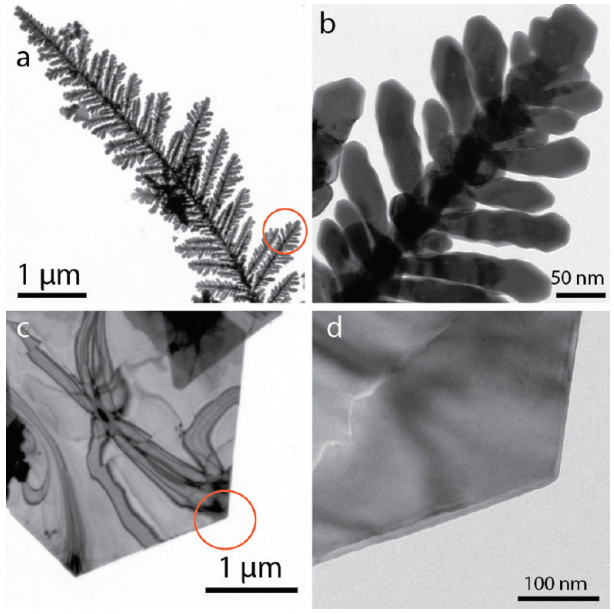

Figure 7. TEM images of (a) Ag dendrite formed after Ag microparticles (>10 μm) were allowed to react with $AgNO_3$ (5 mM) for 5 min. (b) Magnified view of the circled area in part a. (c) Ag nanodisk obtained by the reaction of copper nanoparticles (500 nm) with 0.1 mM $AgNO_3$ for 10 min. The ribbons and lines are the contour lines from the nanodisk bending. (d) Magnified view of the circled area in part c.

the cell potential dropped further to 0.18 V, and when copper particles were allowed to react with a 5 mM solution of $[Ag(S_2O_3)]^{2-}$, the silver was found to deposit uniformly on the surface of copper microparticle (Figure 5b) and nanowire (Figure 5c) to form core–shell structures. No Ag nanobelts and nanodisks protruding from the copper surface were found. Thus, it is clear that lowering the cell potential results in silver nanostructures closer to the copper surface with lower dimensionality. This trend can be applied as a useful guide for the synthesis of heterogeneous metallic nanostructures by galvanic displacement reactions. For example, Xia's group has synthesized Au nanocages when reacting silver nanocubes with $HAuCl_4$.[39,40] The silver nanostructures synthesized in this paper can also be used to react with $HAuCl_4$, forming the Au shell (see Figure S7 in the Supporting Information). (In this case, the potential difference between $AuCl_4^-$ and Ag is 0.2 V, similar to the potential difference between $[Ag(S_2O_3)]^{2-}$ and copper.)

The size of the initial copper particle also affects the nature of the Ag nanostructure formed (Figure 6). When the copper nanoparticle approaches bulk size (10 μm), the silver growth is fast and kinetically controlled, resulting in classical dendritic structures. When the copper particles are smaller (<1 μm), the reaction is slower and more thermodynamically controlled, and nanobelts with lower surface energies are formed. When the copper nanoparticle size is less than 100 nm, the copper nanoparticle is simply converted to a polyhedral silver nanoparticle, which has the lowest surface energy of all (Figure 6a and Figure S5 in the Supporting Information).

The silver dendrites and nanodisks were also characterized using TEM (Figure 7). The diffraction patterns were exactly the same as that for the Ag nanobelt shown in Figure 2c. Although the Ag dendrites and Ag nanodisks appear to have dramatically different structures, careful examination reveals that the branches of the dendrites are similar to short nanobelts, while the tips resemble the nanodisks. These structural similarities are consistent with the different silver nanostructures developing from very similar silver seed crystals during their early growth stages.

Finally, we have attempted to capture the initial stage of silver formation by the reaction of a copper nanowire (200 nm in diameter) with a low concentration of $AgNO_3$ (0.1 mM) for a short time (10 s). Figure 8a shows the TEM image of a small Ag nanodisk on the surface of copper nanowire. Parts b and c of Figure 8 show the EDS mapping of Ag and Cu, respectively, which confirms the protruding Ag growth on the copper surface. We have also studied the process of nanodisk growth by controlling the reaction time of copper nanowire in low

dx.doi.org/10.1021/cm2017714 | Chem. Mater. 2012, 24, 48–54

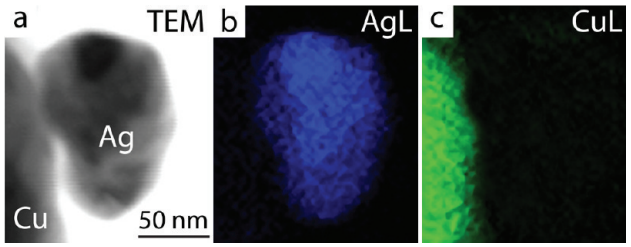

Figure 8. (a) TEM image of initial growth of Ag on a template synthesized copper nanowire. (b and c) Ag and Cu EDS mapping of selected area in part a.

concentration of Ag nitrate. (Figure S6 in the Supporting Information.)

The same growth pattern for Ag is observed even when the copper nanoparticle size is decreased to less than 50 nm. Figure

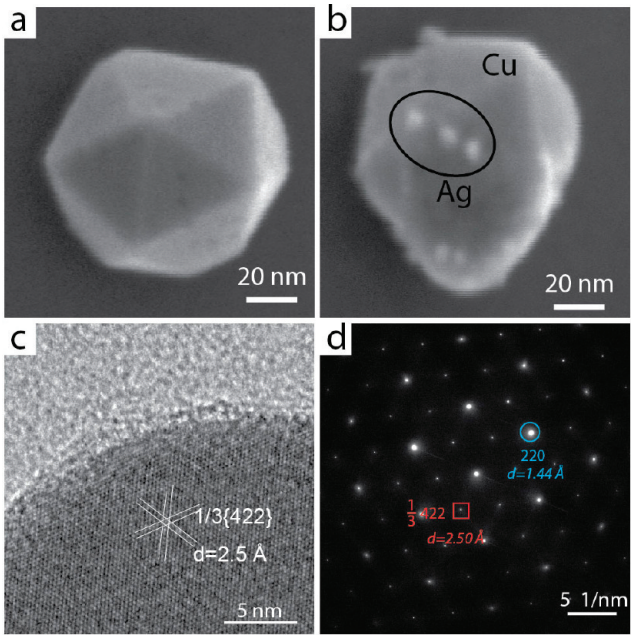

Figure 9. Formation of Ag seed on a small Cu nanoparticle (50 nm). (a) Clean Cu nanoparticles, (b) after reaction with $AgNO_3$ (0.01 mM) for 10 s. (c) High resolution TEM image of the Ag seed. (d) Electron diffraction pattern from the edge of the Ag seed in part c.

9 shows the growth of tiny Ag seeds on a 50 nm copper nanoparticle. Interestingly, the Ag nanoseeds grow preferentially on the edges and vertices of the copper polyhedral nanoparticles, presumably because of the higher surface energy and reactivity of copper atoms on these sites. TEM analysis reveals that the Ag seeds share the same crystal structure and electron diffraction pattern of the Ag nanobelts (Figure 2b and c), as well as those of the initial Ag nanocrystals shown in Figure 10.

Although different Ag nanostructures can be formed under different conditions, the initial Ag seed crystals formed on the copper surface share similar features: 2-D disk shape with a protruding tip (Figure 10a and b and Figure S7 in the Supporting Information). The electron diffraction pattern reveals that the crystal structure of the initial Ag nanocrystal is exactly the same as that observed for the various Ag nanostructures formed subsequently (e.g., Figure 2c). Thus, very similar Ag seed crystals give rise to all the observed

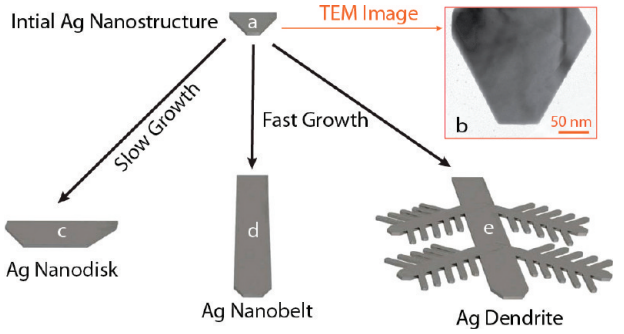

Figure 10. (a) Initial Ag nanocrystal grown on the copper nano/microparticle. (b) Typical TEM image of the Ag nanocrystal grown on the copper particle. (5 mM $AgNO_3$ was allowed to react with 500 nm Cu nanoparticle for 2–3 s; Ag nanobelt was formed ultimately.) (c) Ag nanodisk, (d) Ag nanobelt, and (e) Ag dendrite grown from the initial Ag seed crystal under different conditions.

nanostructures (Figure 10). The final structure depends on the growth rate. The slow, thermodynamically controlled, reaction allows the deposition of Ag on all of the edge of the initial Ag nanocrystal forming a Ag nanodisk (Figure 10c). The nanodisk formation is due to the selective Ag deposition on the lateral surfaces rather than the basal (111) surface of the initial Ag seed. The latter (111) surface has the lowest surface energy for face-center cubic (fcc) crystals. This mechanism is similar to that suggested by Sun et al.[9,34,35] The fast, kinetically controlled, reaction results in more asymmetric structures like nanobelts and dendrites (Figure 10d and e).

■ CONCLUSION

In conclusion, we have found that silver nanostructures, such as Ag nanobelts, can be formed by galvanic displacement reaction without the aid of templates. The growth of these Ag nanostructures is initiated by short-circuited nanobatteries composed of copper nano/microparticles and protruding Ag seeds on their surfaces. The nature and size of the nanostructures Ag formed can be tuned by systematic variation in cell potential for the galvanic displacement reaction (e.g., by changing the identity and concentration of the starting silver(I) species) and size of the starting copper nano/microparticle. Higher cell potentials lead to kinetic control of the reaction and the formation 1-D silver nanobelts protruding from the copper surface. Lower cell potentials lead to more thermodynamic control and the formation of 2-D Ag nanodisks or even Ag nanoshells that are closer to the copper surface. The various silver nanostructures share analogous structural features because they develop from very similar silver seed crystals during their early growth stage.

The Ag nanostructures synthesized in this report may find interesting applications. For examples, 2-D Ag nanodisks can be spread on a surface to fabricate cost-effective surface enhanced Raman spectroscopy (SERS) substrates.[32] 1-D Ag nanobelts can be coated on a substrate and can serve as conductive nanoelectrodes.[27−29] More complicated architectures may be attained by using the Ag nanostructures as "templates." For example, the subsequent reaction of aqueous $HAuCl_4$ results in uniform coating the silver structures with gold (Figures S8 and S9 in the Supporting Information).

dx.doi.org/10.1021/cm2017714 | Chem. Mater. 2012, 24, 48−54

EXPERIMENTAL SECTION

Chemicals and Materials. Large copper nanoparticles (0.5 to 10 μm) are commercially available from Alfa Aesar. Copper nanorods (~200 nm in diameter) were made by template synthesis. Small copper nanoparticles (~50 nm), shown in Figures 6a and 9, were electrochemically synthesized on a silicon wafer. Copper nanoparticles (20 nm), shown in Figure S5 in the Supporting Information, were obtained from American Elements. Silicon wafer (5 mΩ-cm, p-type, ⟨100⟩ crystal orientation) was purchased from Silicon Quest. Alumina template with 200 nm pore size is commercially available from Whatman. Carbon film supported gold TEM grids (200 mesh) were purchased from Electron Microscope Sciences. Ethanol, silver nitrate, chloroauric acid, potassium silver cyanide, copper sulfate, diethlenetriamine, ammonium sulfate, ammonium persulfate, sodium perchlorate, hydrogen fluoride, silver chloride, sodium thiosulfate, copper foil (99.99%), and silver foil (99.99%) were obtained from Sigma Aldrich. Silver thiosulfate was prepared by dissolving 5 mM silver chloride in 40 mM sodium thiosulfate. Deionized water was made by a Barnstead Nanopure Diamond Water system. All chemicals were used as received, and all the solutions were freshly prepared.

Synthesis. Silver nanostructures: Copper nanoparticles or nanorods were first dispersed in pure ethanol. The suspension was dropped on the surface of silicon wafer or indium tin oxide glass (these conductive substrates facilitate the SEM observation) and allowed to dry out. Then, the silver nitrate solution was added to grow the silver nanostructures. After the reaction was completed, the silver nitrate solution was removed using Kimwipes. The resulting silver nanostructures were repeatedly rinsed with copious amounts of water.

Copper nanorods: An alumina template was sputtered with copper (200 nm) using Kurt Lesker CM-18/RF sputtering system. Copper nanorods were synthesized potentiostatically (−1.1 V) in the copper sputtered alumina template from a solution of copper sulfate (100 g/L), diethylenetriamine (80 mL/L), and ammonium sulfate (20 g/L)[43] on the potentiostat SP-150 from Biologic. Typically, 1.5 C is passed on the 0.3 cm^2 alumina template for the electrochemical deposition of copper nanorods. All potentials were measured relative to an Ag/AgCl reference electrode, using a platinum foil as a counter electrode, if not specified otherwise. The back sputtered copper was etched by 50 mM ammonium persulfate solution. The alumina template was subsequently removed by 3 M NaOH solution to release the copper nanorods. The obtained copper nanorods were centrifuged and washed repeatedly at least 8 times and finally dispersed in ethanol. Silver was electrodeposited in a similar way as copper (−0.6 V, from the solution of potassium silver cyanide 60 g/L).

Copper Nanoparticles (50 nm): Copper nanoparticles (50 nm) were electrochemically synthesized on the silicon wafer from a solution consisting of 10 mM copper sulfate and 10 mM sodium perchlorate by applying −1.1 V for 3 s. Before the electrodeposition, the silicon wafer was briefly treated with 5% HF to remove the silicon oxide.

Characterizations. Optical imaging of the silver nanobelts growth was done using a Zeiss-Axiovet 200 inverted optical microscope with HITACHI KPD20BU camera. PhysVis AVI video analysis software (by David M. Cowart and Timothy S. Sullivan) was used to analyze the dynamic growth process of silver nanobelts. SEM images were obtained using the Leo 1530 field emission scanning electron microscope at 3 kV. TEM images (including the high resolution TEM images, SEAD, and EDS analysis) were collected by JEOL 2010F field emission TEM/STEM with EELS and EDS at 200 kV. The preparation of the TEM samples was done by reacting copper nanoparticles/nanorods with silver nitrate on the Au/Ni TEM grid. The cell potential difference is measure by the potentiostat SP-150 from Biologic using the open-circuited method.

ASSOCIATED CONTENT

Supporting Information

SEM and TEM images and Ag nanobelt growth video. This material is available free of charge via the Internet at http://pubs.acs.org.

AUTHOR INFORMATION

Corresponding Author

*E-mail: asen@psu.edu.

ACKNOWLEDGMENTS

We gratefully acknowledge funding by the U.S. Department of the Army through MURI Grant No. W911NF-06-1-0280. We deeply appreciate Dr. Joe Kulik for his help with TEM imaging and analysis.

REFERENCES

(1) Sun, Y. G.; Xia, Y. N. *Adv. Mater.* **2002**, *14*, 833.
(2) Jana, N. R.; Gearheart, L.; Murphy, C. J. *Chem. Commun.* **2001**, 617.
(3) Kline, T. R.; Tian, M. L.; Wang, J. G.; Sen, A.; Chan, M. W. H.; Mallouk, T. E. *Inorg. Chem.* **2006**, *45*, 7555.
(4) Sauer, G.; Brehm, G.; Schneider, S.; Nielsch, K.; Wehrspohn, R. B.; Choi, J.; Hofmeister, H.; Gösele, U. *J. Appl. Phys.* **2002**, *91*, 3243.
(5) Liu, B. Q.; Luo, W.; Zhao, X. P. *Mater. Res. Bull.* **2009**, *44*, 682.
(6) Caswell, K. K.; Bender, C. M.; Murphy, C. J. *Nano Lett.* **2003**, *3*, 667.
(7) Sun, Y. G.; Gates, B.; Mayers, B.; Xia, Y. N. *Nano Lett.* **2002**, *2*, 165.
(8) Yan, H.; Park, S. H.; Finkelstein, G.; Reif, J. H.; LaBean, T. H. *Science* **2003**, *301*, 1882.
(9) Sun, Y. G. *Adv. Funct. Mater.* **2010**, *20*, 3646.
(10) Maillard, M.; Giorgio, S.; Pileni, M. P. *Adv. Mater.* **2002**, *14*, 1084.
(11) Sun, Y. G.; Xia, Y. N. *Adv. Mater.* **2003**, *15*, 695.
(12) Chen, S. H.; Fan, Z. Y.; Carroll, D. L. *J. Phys. Chem. B* **2002**, *106*, 10777.
(13) Maillard, M.; Huang, P. R.; Brus, L. *Nano Lett.* **2003**, *3*, 1611.
(14) Lai, Y. C.; Pan, W. X.; Zhang, D. J.; Zhan, J. H. *Nanoscale* **2011**, *3*, 2134.
(15) Wang, L.; Clavero, C.; Huba, Z.; Carroll, K. J.; Carpenter, E. E.; Gu, D. F.; Lukaszew, R. A. *Nano Lett.* **2011**, *11*, 1237.
(16) Jackson, J. B.; Halas, N. J. *J. Phys. Chem. B* **2001**, *105*, 2743.
(17) Qu, L. T.; Shi, G. Q.; Wu, X. F.; Fan, B. *Adv. Mater.* **2004**, *16*, 1200.
(18) Bai, J. W.; Qin, Y.; Jiang, C. Y.; Qi, L. M. *Chem. Mater.* **2007**, *19*, 3367.
(19) Liu, S. W.; Wang, W. Z.; Zhou, L.; Zhang, L. S. *J. Cryst. Growth* **2006**, *293*, 404.
(20) Deng, Z. T.; Mansuipur, M.; Muscat, A. J. *J. Phys. Chem. C* **2009**, *113*, 867.
(21) Huang, T. K.; Cheng, T. H.; Yen, M. Y.; Hsiao, W. H.; Wang, L. S.; Chen, F. R.; Kai, J. J.; Lee, C. Y.; Chiu, H. T. *Langmuir* **2007**, *23*, 5722.
(22) Aizawa, M.; Cooper, A. M.; Malac, M.; Buriak, J. M. *Nano Lett.* **2005**, *5*, 815.
(23) Sun, Y. G.; Mayers, B.; Xia, Y. N. *Nano Lett.* **2003**, *3*, 675.
(24) Tao, F.; Wang, Z. J.; Chen, D. B.; Yao, L. Z.; Cai, W. L.; Li, X. G. *Nanotechnology* **2007**, *18*, 295602.
(25) Reches, M.; Gazit, E. *Science* **2003**, *300*, 625.
(26) Nicewarner-Pena, S. R.; Freeman, R. G.; Reiss, B. D.; He, L.; Pena, D. J.; Walton, I. D.; Cromer, R.; Keating, C. D.; Natan, M. J. *Science* **2001**, *294*, 137.
(27) De, S.; Higgins, T. M.; Lyons, P. E.; Doherty, E. M.; Nirmalraj, P. N.; Blau, W. J.; Boland, J. J.; Coleman, J. N. *ACS Nano* **2009**, *3*, 1767.
(28) Hu, L.; Kim, H. S.; Lee, J.-Y.; Peumans, P.; Cui, Y. *ACS Nano* **2010**, *4*, 2955.
(29) Yu, Z.; Zhang, Q.; Li, L.; Chen, Q.; Niu, X.; Liu, J.; Pei, Q. *Adv. Mater.* **2010**, 664.
(30) Gutes, A.; Carraro, C.; Maboudian, R. *ACS Appl. Mater. Interfaces* **2009**, *1*, 2551.

(31) Zhang, B.; Xu, P.; Xie, X. M.; Wei, H.; Li, Z. P.; Mack, N. H.; Han, X. J.; Xu, H. X.; Wang, H. L. *J. Mater. Chem.* **2011**, *21*, 2495.
(32) Gutes, A.; Carraro, C.; Maboudian, R. *J. Am. Chem. Soc.* **2010**, *132*, 1476.
(33) Sun, Y. *Nanoscale* **2011**, *3*, 2247.
(34) Sun, Y. *J. Phys. Chem. C* **2009**, *114*, 857.
(35) Sun, Y. *Chem. Mater.* **2007**, *19*, 5845.
(36) Wang, C. Y.; Lu, M. Y.; Chen, H. C.; Chen, L. J. *J. Phys. Chem. C* **2007**, *111*, 6215.
(37) Xiao, F.; Yoo, B.; Lee, K. H.; Myung, N. V. *J. Am. Chem. Soc.* **2007**, *129*, 10068.
(38) Liu, L.; Yoo, S. H.; Park, S. *Chem. Mater.* **2010**, *22*, 2681.
(39) Skrabalak, S. E.; Chen, J. Y.; Sun, Y. G.; Lu, X. M.; Au, L.; Cobley, C. M.; Xia, Y. N. *Acc. Chem. Res.* **2008**, *41*, 1587.
(40) Chen, J.; Saeki, F.; Wiley, B. J.; Cang, H.; Cobb, M. J.; Li, Z. Y.; Au, L.; Zhang, H.; Kimmey, M. B.; Li, X. D.; Xia, Y. *Nano Lett.* **2005**, *5*, 473.
(41) Germain, V.; Li, J.; Ingert, D.; Wang, Z. L.; Pileni, M. P. *J. Phys. Chem. B* **2003**, *107*, 8717.
(42) Jin, R. C.; Cao, Y. W.; Mirkin, C. A.; Kelly, K. L.; Schatz, G. C.; Zheng, J. G. *Science* **2001**, *294*, 1901.
(43) Taberna, L.; Mitra, S.; Poizot, P.; Simon, P.; Tarascon, J. M. *Nat. Mater.* **2006**, *5*, 567.